Influence of anthopometric variables on the mechanical properties of human rib cortical bone

Juan Velázquez-Ameijide[a] · Silvia García-Vilana[a] · David Sánchez-Molina[a], · Eva Martínez-González[a] · Jordi Llumà[b], · M.Carmen Rebollo-Soria[c] · Carlos Arregui-Dalmases[d]

Abstract *Objective.* The mechanical properties of ribs from a large number of *post-mortem* human subjects (PMHS) were analyzed to search for variation according to age, sex or BMI in the sample. A large sample of specimens from different donors ($N = 64$) with a very wide range of ages and anthropometric characteristics was tested.

Methods. Uniaxial tensile tests were used for a sample of coupons machined from cortical bone tissue in order to isolate the purely mechanical properties from the geometrically influenced properties of the rib. Each coupon is about 25 mm long and has a thickness of about 0.5 mm. The mechanical properties measured for each specimen/coupon include YM, yield stress, ultimate stress (maximum failure stress), ultimate strain, and resilience (energy to fracture of SED). The study provides new methodological improvements in DIC techniques.

Results. This study is notable for using an atypically large sample of number of PMHS. The size of the sample allowed the authors to determine that age has a significant effect on failure stress ($p < 0.0001$), yield stress ($p = 0.0047$), ultimate strain ($p < 0.0001$) and resilience ($p < 0.0001$) [numbers in parentheses represent the corresponding $p-$values]. Finally, there is a combined effect, so that for a given age, an increase of BMI leads to a decrease of the maximum strain (i.e. cortical bone is less stiff when both age and BMI are higher).

Nomenclature
BMI - Body Mass Index

[a]UPC, EEBE-GRABI, Eduard Maristany, 14, 08019 Barcelona
[b]UPC, EEBE-PROCOMAME, Eduard Maristany, 14, 08019 Barcelona
[c]IMLA-Subdirección de Huesca, Irene Izárbez, 2, 22005 Huesca
[d]Centro Zaragoza, Crtra. 232, km.273, 50690 Pedrola

DIC - Digital Image Correlation
MAIS - Maximum in the Abbreviated Injury Scale
MVCs - Motor Vehicle Crashes
PMHS - Post mortem Human Subject
ROI - Region of Interest
SED - Strain Energy Density
YM - Young Modulus

1 Introduction

Thorax injuries are frequent in MVCs of different types (frontal impacts, side impacts or vehicle pedestrian collisions). For the occupants of the vehicle, a study detected that in crashes with at least one injured person: 19% of occupants are uninjured, 49% of occupants sustain MAIS 1 injuries, 15% MAIS2, 8% MAIS 3, and 9% MAIS 4+. In this sample, the body regions most often injured are head, upper and lower extremities and thorax; specifically, in the thorax injuries 23% of the injured people presented MAIS1 injuries, and 11% MAIS2 [1]. Thoracic injuries are the most frequent after head injuries in terms of the number of fatalities and serious injuries in MVCs [2], and are the most frequent injuries in motorbike-pedestrian collisions [3]. The data of estimated Disability Risk (DR) show that older adults had significantly greater overall disability than each of the other age groups, the average DR varies from $50.0 \pm 15.4\%$ for older adults to $29.0 \pm 13.7\%$ for pediatric patients, in all the age groups of adults the DR $> 30\%$ [4].

In studies of human ribs, different testing methods have been used such as three-point bending tests [10–12]. Most of these studies use the entire rib, but as it was explained above, such methododology mixes intrinsic and extrinsic properties. Nevertheless, there are some recent works focused on the manufacturing of coupon specimens that allowed to isolate the material properties from the geometric component of the entire rib. Two recent studies that perform quasi-static and dynamic tests with a similar methodology used in this study are comparable with the present study [13,14]. These last two studies interestingly reached many similar conclusions to the present study, even using some methodological differences.

Because of the above reasons, this research aims to provide a new set of data, reviewing the method to manufacture human rib cortical bone coupons for consistent, reliable material testing, without defects and with a high control on the thickness of the specimens. Additionally, some methodological innovations in the fixtures and the computation of strains are proposed, which can be useful in similar testing procedures. The mechanical properties of human rib cortical bone obtained are investigated in order to assess the influence of various anthropometric and age-related factors, using a large-enough sample size to quantify the statistical significance of those factors. Although some

relatively old studies did not find significant decreasing of the mechanical properties with age [15], these studies had a small subject sample sizes, ranging from three to six subjects. Studies with a greater number of samples found significant reductions in mechanical properties in the elastic modulus, yield stress, failure stress and failure strain for advanced age.

2 Methods

In this study, eighty-three human cortical bone coupons were obtained from the anterior and lateral regions of ribs from 64 deceased donors. The specimen preparation, the tensile testing configuration, the data processing and the statistical methodology are described below. The obtained data will then be analyzed to assess the influence of the anthropometric properties on the mechanical properties of the ribs.

2.1 Material

The test material used in this study were specimens of human rib cortical bone, harvested from forensic autopsies at the Forensic Pathology Service of the Legal Medicine and Forensic Science Institute of Catalonia (IMLCFC) which were initially removed for complementary medico-legal investigation. This study was approved by the Research and Ethics committee of IMLCFC. Specimens were harvested from the 7th rib from 64 different deceased donors (44 male and 20 female), with an average age of 55 years (ranging from 10 to 91 years) and a mean BMI of 29 kg/m^2. The donors were categorized by age, with age ranges defined such that each range included between five and ten donors. This allowed to perform a statistical analysis by age category (Table 1). Only donors with a known cause of death were used: trauma, cancer or indefinite causes were excluded from the sample.

Table 1 Donors characteristics divided in age ranges.

Age range (y.o.)	Males	Females	Height [cm]	Weight [kg]	BMI [kg/m^2]
10-29	6	0	169.2±3.1	72.2±4.6	25.2 ± 1.5
30-35	6	2	170±2.3	82.9±5.5	28.8 ± 5.2
36-40	5	1	160.7±4.3	71.5±3.5	27.7 ± 0.8
41-50	5	2	167.9 ± 3.2	86.9 ± 4.3	30.9 ± 1.4
51-60	5	1	168 ± 4.2	83.2 ± 6.4	30 ± 3.3
61-65	5	4	161.7 ± 1.7	77.2 ± 4.8	29.5 ± 1.8
66-70	3	2	163.6 ± 5.9	85 ± 8.5	32.2 ± 4.1
71-80	4	4	158.5 ± 3.7	74.8 ± 7.3	29.5 ± 2.5
81-91	5	4	154.6 ± 3.3	65.6 ± 4.8	27.6 ± 2.2

2.2 Specimen preparation

Once received, the specimens were wrapped in saline soaked gauze and stored in air-lock plastic bags in a freezer at a temperature of –20°C. Previous studies showed that the storage of bone specimens at –20°C does not modify the properties of the specimen. Before sample machining, the specimens were defrosted in a fridge at 5°C [16,17]. Bone coupons were machined from entire ribs, following the method described in previous studies [14,18]. First, soft tissue was removed (Fig. 1 (a)) and then the rib was divided in different parts (Fig. 1 (b))
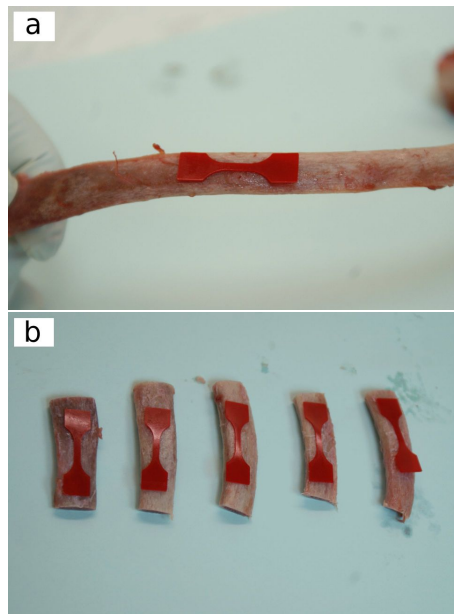

Fig. 1 Location of the coupons on the rib (a) and rib sections for coupon manufacturing (b).

Each obtained portion was then glued on a polymer fixture and attached to the specimen holder of a low speed diamond saw (Fig. 2 (a)). Using the low-speed diamond saw, slices of cortical bone from the cutaneous surface of the rib were cut away from the specimen (Fig. 2 (b)).

In each bone slice, two drill holes of 2 mm in diameter were drilled, being spaced 20 mm apart (Fig. 3 (a)). These holes allowed for the centering and fixation of the samples during the machining and in the clamping system of the tensile test. Then, each slice was machined with a milling machine and a pattern in order to obtain the coupon geometry (Fig. 3 (b,c)).
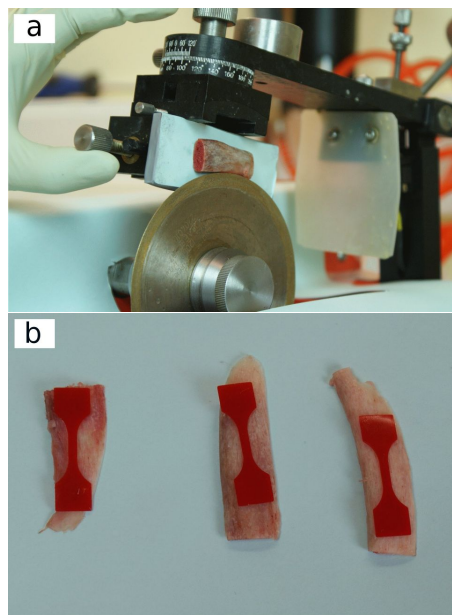
Fig. 2 Rib section cutting process to obtain a cortical bone slice (a) and cortical bone slices obtained (b).
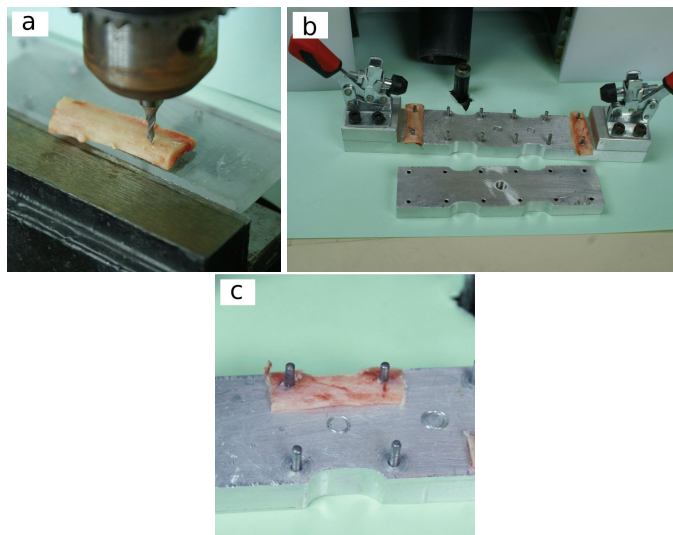

Fig. 3 Drilling of the bone slice (a), assembly of the slice on the machining tool (b), and coupon sample with half geometry machined (c).

Finally, each sample was polished using an aluminum tool with a groove of 0.5 mm that allowed the control of the final thickness of the coupon (Fig. 4 (a)). The thickness and width of the gauge length of the sample were carefully

determined in order to obtain the accurate value of the cross-sectional area of
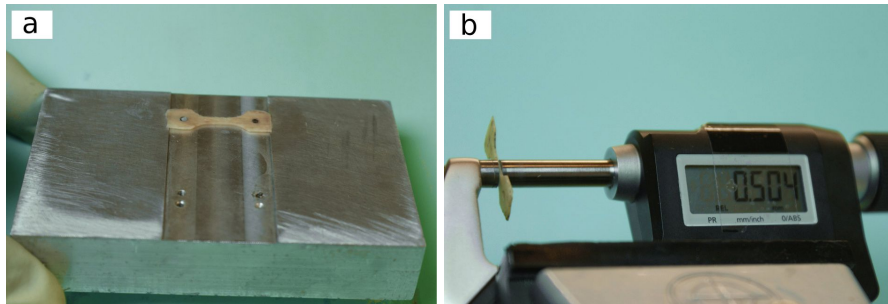the specimen (Fig. 4 (b)).

Fig. 4 Coupon assembled on the polishing tool (a), and coupon thickness measurement
(b).

2.3 Tensile test

Tensile tests were performed with a MicroTEST® EM2/20, and a load cell
of 500 N, coupled with a data acquisition system (Spider 8-30 from HBM®)
with a frequency of data acquisition of 60 Hz. The coupon sample was fixed in
two special clamping jaws. Special tools were designed for the attachment of
the jaws in the tensile machine without breaking the sample (Fig. 5 (a)). Once
the sample was assembled in the jaws, the upper jaw was attached directly to
the load cell, and an eyebolt was fixed in the lower jaw. In the lower base of
the tensile machine, a polymeric tooling with two holes was attached. A pin
was then inserted into these holes and within the eyebolt of the clamping jaw
(Fig. 5 (b)). This system constrains the movement of the sample during the
test.
All tests were recorded with a high-definition camera. The camera was set up
to obtain a full video of the gauge length during the entire test. The samples
were painted with a pattern of random black dots of spray-paint. The video
recordings were later used with DIC (see section 2.4) to determine the strain
time histories during the tests (Fig. 5 (c)). The sampling rate for the video is
60 fps.
All samples were loaded to failure at a strain rate of $\dot{\varepsilon} = 0.0138 \text{ s}^{-1}$ to ensure
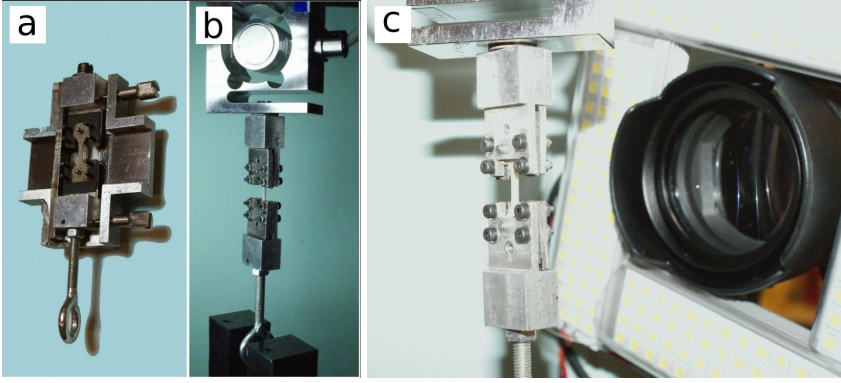quasi-static conditions and enough data acquisition before the fracture.

Fig. 5 Coupon assembling in the jaws (a), assembly mounted on the tensile test machine (b), and camera positioning for the video recording during the tensile test (c).

2.4 Data processing and Digital Image Correlation

The recorded video during the test was decompressed (broken down) into frames. To process these frames, a Digital Image Correlation and Tracking software package [19] in MATLAB® (DIC) was used. This software had been used in previous similar studies for measuring strain during uniaxial tensile tests [14,18]. Once the frames of interest (FOI) were chosen (i.e. the frames ranging from the beginning of the test until sample fracture), a grid of 50×50 pixels was defined on the gauge length of the sample in the first FOI (Fig. 6). A script was used to determine the pixel intensity (i.e. the color of the gray scale of the pixel) that surrounded each point of the grid. Then, the script searched the new position of each point in the next frame, by looking for the most similar pixel intensity. After the preliminary identification of the points of the grid from one frame to the following frame, some corrections were implemented, because in the experimental setting there is no rigid fixation of the ends, some specimens may experience slight re-positioning (rotation on three axes, slight approaching or moving away from the recording device). Due to the high number of points in the grid (about 200 points are used), the redundancies can be used to separate re-positioning from mechanical deformation. This is achieved by estimating whether there are rotations or approaches to the focus of the recording device. For each point of the grid, the change in coordinates of a point between a frame and the previous one is related by a combination of refocusing $\mathbf{H}_\delta$, rotations around the three axes $\mathbf{R}_\alpha^X, \mathbf{R}_\beta^Y, \mathbf{R}_\gamma^Z$ and real physical deformation $\mathbf{F}$:

$$\mathbf{u}_n = \mathbf{R}_Z^\gamma \mathbf{R}_Y^\beta \mathbf{R}_X^\alpha \mathbf{H}_Z^\gamma \bar{\mathbf{u}}_n \tag{1}$$

in this equation, the coordinates $\bar{\mathbf{u}}_n(x,y,z)$ are the apparent positions (as are directly found with the unimproved software), and for each frame the parameters $\alpha, \beta, \gamma, \delta$ are estimated, resulting always small values, and then the corrected position $\mathbf{u}_n(x,y,z)$ is computed. This step was repeated for each point and in each frame. Hence, knowing the position of the points in
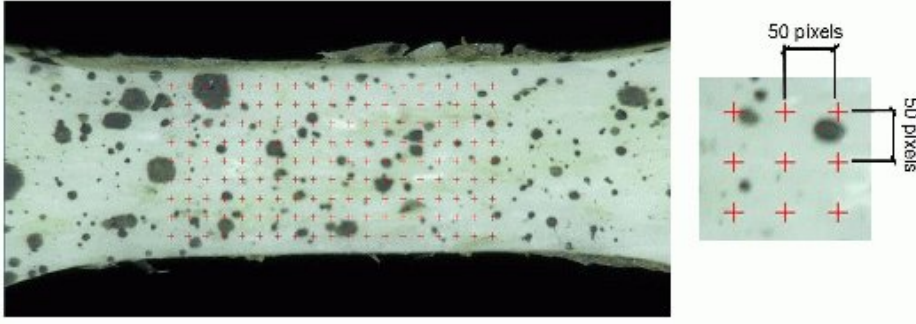
Fig. 6 A generated grid (with 9×17 reference points) on the gauge length of the coupon with the Digital Image Correlation and Tracking software.

each frame, elongations could be determined and strain calculated (Figure 7 compares the strain maps obtained from the uncorrected positions and the strain map with corrections in equation (1)). Finally, Finite Strain Theory can be applied once the positions of the points on the grid have been determined for each frame. In particular, the *Green-Lagrangian strain* components can be computed by means of the following equation:

$$E_{ij} = \frac{1}{2} \left(\frac{\partial u_i}{\partial x_j} + \frac{\partial u_i}{\partial x_j} + \sum_{k=1}^{3} \frac{\partial u_k}{\partial x_i} \frac{\partial u_k}{\partial x_j} \right) \tag{2}$$

for $i, j \in \{1, 2\}$ [being $x_1 = x$ and $x_2 = y$]. In practice, the values of the derivatives $\partial u_i / \partial x_j$ are obtained by means of a regression analysis at each step, computing the slope of the curves of displacement $u_i(x, y, z)$.
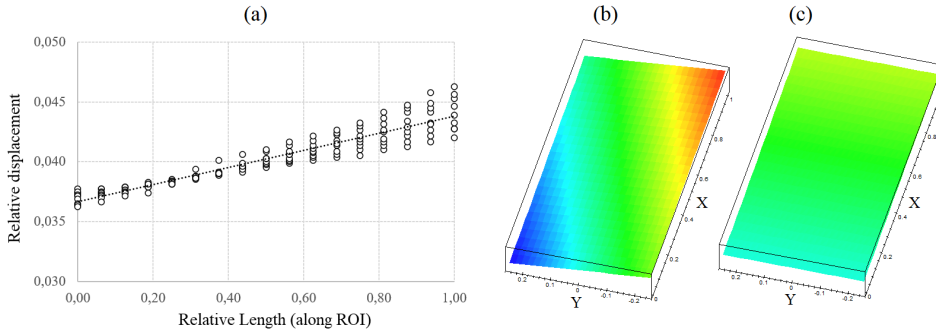

Fig. 7 Computation of strains: (a) displacement field in step $n = 2000$, $\mathbf{u}_{2000}$ ($t = 33.3$ s): infinitessimal strain ε is the slope the straight line, (b) strain map associate with the uncorrected displacements (a rotation around X axis distorts the real strain field), (c) corrected strain map eliminating the X rotation by means of equation (1), the real strain field in the ROI must be uniform.

This method for calculating strain has some computational complexity, but it is very robust and easy to perform in a conventional computer. In addition, since there are 60 frames-per-second in the video recording, the results are very accurate. Indeed, the curves directly obtained are so smooth that it is not necessary to use any additional filtering, as it can be appreciated in Figures 8 to 12. One of the advantages of this methodology is that with very small changes it can be applied to the entire rib tests with very good accuracy.

2.5 Statistical analysis

The influence of sex, age, and BMI of the individuals on the mechanical properties were analyzed by using the XLSTAT® statistical package. Two kinds of analyses were performed; a fitting to a distribution of all the values for each mechanical property to determine how the data were distributed, and a regression analysis, with the aim of providing a descriptive model where the influence of anthropometric factors is observed in each property. In the regression analysis, the obtained residual have been tested for normality (Shapiro–Wilk test) and homoscedasticity (Breusch–Pagan test). In the regression analysis, p-values have always been used to verify if the effects were significant, previously checking that the residues obtained followed a normal distribution.

A second level statistical analysis was implemented to evaluate the influence of anthropometric variables (i.e., age, sex and BMI) on the mechanical properties. Results are presented in Table 3, with α_0 being an outcome value whose units are the same as the property evaluated. Sex is codified as 0 if the subject is male or 1 if it is female.

3 Results

From the 64 ribs, eighty-three coupon test specimens were obtained. In all the coupons fracture occurred within the gauge length. For each of the coupons, the following properties were determined: failure stress, maximum strain, yield strength, YM and fracture energy (Fig. 2). The results od the tests are presented in Fig. 8-12 and Table 2.

Note that, since Figures 8 to 12 are intended to show the range of YM values of each age group and the overall trends, these figures have been shown in a windowed strain range that allows to clarify and distinguish the results. The strain range for each age group is shown in Table 2.

Table 2 Mechanical properties divided in age ranges.

Age (y.o.)	σ_{max} [MPa]	e_{max} [%]	E [GPa]	$\sigma_{0.2}$ [MPa]	$W_{fracture}$ [kJ/m^3]
10-29	150 ±10.1	2.23 ± 0.4	15.1 ± 0.9	119.1 ± 7.7	2.57 ± 0.7
30-35	154.8±12	2.28 ± 0.4	20 ± 1.4	131.3 ± 5.9	2.85 ± 0.6
36-40	151.1 ± 16.1	2.26 ± 0.7	16.6 ± 2.4	126.5 ± 10.9	2.83 ± 1.2
41-50	142.3 ± 8.5	2.06 ± 0.4	16.6 ± 0.7	118.8 ± 10	2.16 ± 0.5
51-60	131.7 ± 11.8	1.88 ± 0.2	14.9 ± 1.2	110.8 ± 10.6	1.85 ± 0.4
61-65	127.3 ± 10.8	1.62 ± 0.2	16 ± 0.8	118.2 ± 6.7	1.64 ± 0.3
66-70	110.6 ± 8.6	1.07 ± 0.2	16.3 ± 1	113.7 ± 1.5	0.84 ± 0.3
71-80	95.8 ± 8.5	0.92 ± 0.1	17.4 ± 2	85.2 ± 10.33	0.58 ± 0.1
81-91	100.5 ± 7.6	1.26 ± 0.2	14.7 ± 1.2	98 ± 7.3	0.91 ± 0.2
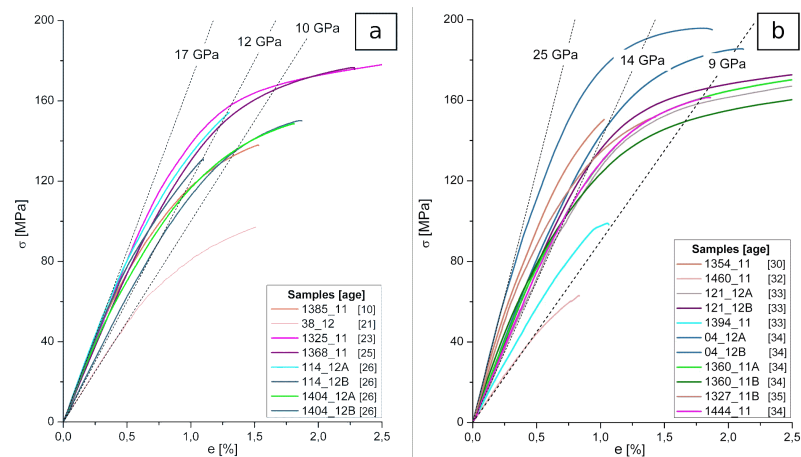
Fig. 8 Tensile stress vs. strain and Young's modulus values of individuals under 29 years (left) and subjects with 30-35 years (right).
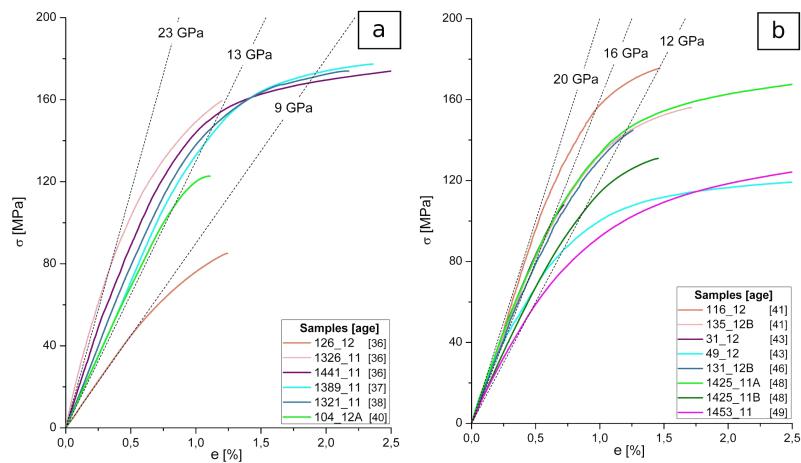
Fig. 9 Tensile stress vs. strain and Young's modulus values of individuals with 36-40 years (left) and subjects with 41-50 years (right).
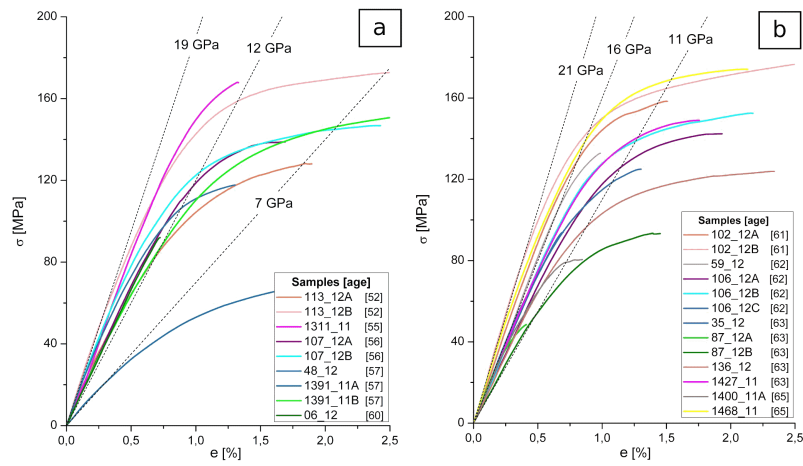
Fig. 10 Tensile stress vs. strain and Young's modulus values of individuals with 51-60 years (left) and subjects with 61-65 years (right).
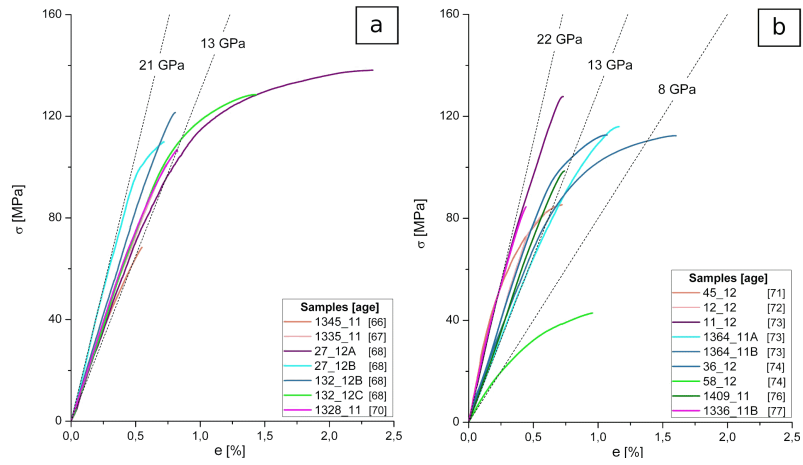

Fig. 11 Tensile stress vs. strain and Young's modulus values of individuals with 66-70 years (left) and subjects with 71-80 years (right).
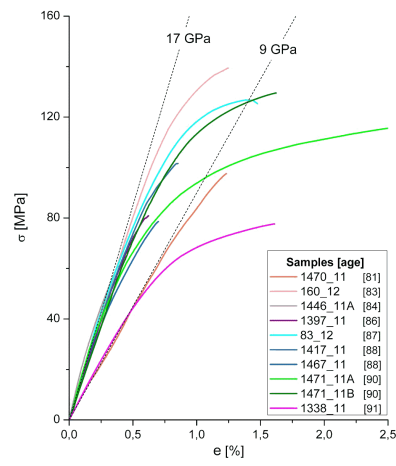
Fig. 12 Tensile stress vs. strain and Young's modulus values of individuals over 81 years

3.1 Age influence

A significant influence has been found between the age of the donors and the failure stress ($p < 0.0001$), yield stress ($p = 0.0047$), maximum strain ($p < 0.0001$) and energy to fracture ($p < 0.0001$). All these properties decreased as age increases. Nevertheless, no age influence on YM was detected (Figs. 13- 15).
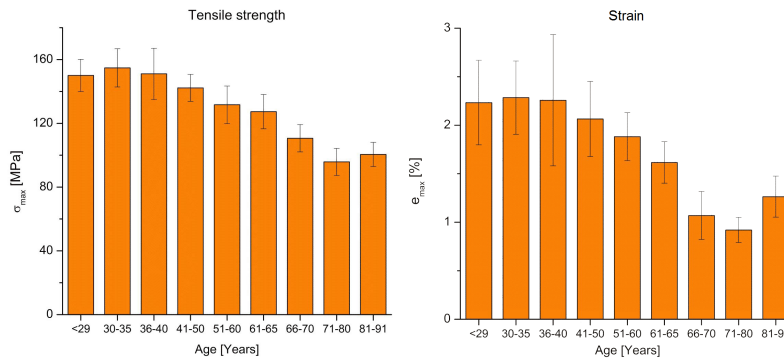

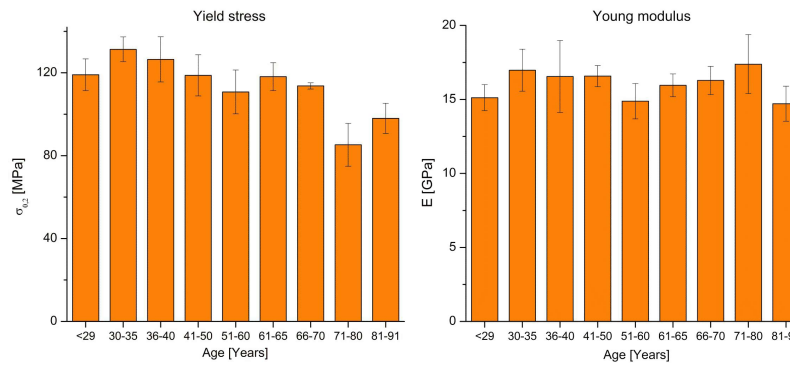**Fig. 13** Influence of age on failure stress and maximum strain

Fig. 14 Influence of age on yield strength and Young's modulus

3.2 Body Mass Index influence

Body Mass Index (BMI) did not show a significant major influence on maximum strain, just a secondary second order was detected. This influence was only observed when BMI was analyzed together with age (the new variable
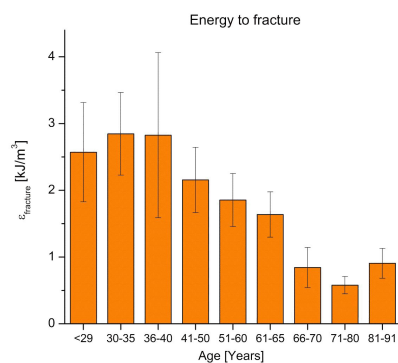
Fig. 15 Influence of age on energy to fracture
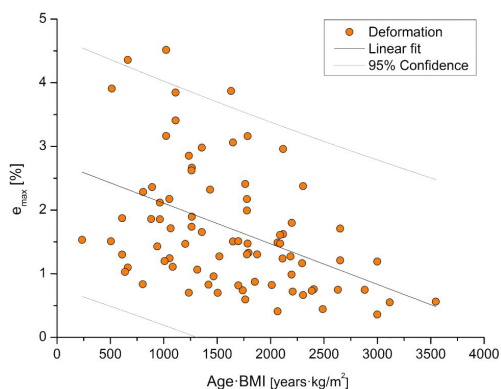
Fig. 16 Combined influence of age and BMI on Failure Stress.

''age · BMI'' has a significant p-value). Between two individuals of the same age, the one with a higher BMI presented a lower elasticity in its bones (Fig. 16).

3.3 Yield stress and Failure Stress

All samples considered in the analysis were loaded to failure and no sample with anomalous breaking was considered in the analysis of any mechanical property. By means of a statistical analysis, a correlation of $r = 0.88$ was found between both parameters, and could be related, following a relation:

$$\sigma_{\max} = 1.2 \; \sigma_{0.2} \tag{3}$$

This suggests that these two properties are related.

4 Discussion

In contrast to other studies that have tested whole ribs in complex loading modes such as bending, the methodology used in this research enabled us to isolate the intrinsic material behavior of the rib cortical bone with uniaxial tension tests.

In the present study, the properties obtained are only dependent on the material behavior of the rib cortical bone, and are not affected by the complex 3D geometry of the bone. Moreover, tensile tests do not require the use of structural mechanics equations that represent the rib as a simplified structural system (such as a beam), which may further introduce error into the calculation of the mechanical properties.

While some authors have performed tensile tests with coupons obtained from human rib cortical bone, drawbacks in the development of this technique had been found in early studies, but some recent studies improved the technique and allowed to find significant relations with anthropometric variables [13,14].

In the present study, a loss in the mechanical capacities of bone with age was found, the sample is one of the largest used in studies of this type ($N = 64$ donors). The findings are similar to the ones found in a recent study based in a sample of $N = 64$ donors, and one of the aims is to analyze the influence of anthropometric variables such as age or sex in the mechanical properties [13]. In our present study, eighty-three coupons of cortical bone of human ribs (from some donors multiple specimens could be obtained), with a wide range of ages and anthropometric characteristics. Only the 7th rib was used so the influence of age, BMI and sex could directly be analyzed disregarding the potential difference of mechanical properties between different rib locations (YM, yield stress, yield strain, failure stress, failure strain, and work to fracture or SED). Due to the high number of individual cadaver specimens available, different regression analyses to determine the effects of variables between individuals could be conducted.

Regarding the mechanical properties, the results showed an average failure stress value of 128.4±4.1 MPa, the above value is similar to the values found in [22,23] and [13]. Moreover, these strength values are in the range of those obtained in three point bending tests by [20], which observed ultimate stress values of 154 MPa, 115.7 MPa and 127.7 MPa for anterior, lateral and posterior regions; and [21], which obtained values of 135.4 MPa testing from the 2nd to 12th rib. However, it is worth noting that two studies used all rib locations within the thorax [20,21], affecting the mechanical property values obtained, which are dependent on the rib under consideration [20]. On the other hand, our values are in the range found by the most recent study [13].

Average Young's modulus values obtained in this study were 16±0.4 GPa and yield strength 115.5±3 MPa, both values are higher than those obtained by Kemper et al. [22], which were 13.9 GPa and 93.9 MPa respectively. Compared with the results obtained in three point bending tests, Young's modulus values obtained in this study were higher. While [10] provided 2.3 GPa for the 7th

rib and 1.89 GPa for the 8th rib, [20] obtained an average modulus of 11.85 GPa for the lateral part and 7.51 GPa for the anterior region. This can be attributed to the different tests performed in those studies, and to the use of a different rib location. The average ultimate strain observed in this study was 1.72±0.12%, which is similar to the values obtained in other studies [22,23]. In the most recent study, Young's modulus ranges 13-17 GPa, in good agreement with our study.

Table 3 Statistical influence of anthropometric variables on mechanical properties (coefficients represent the expected change in mechanical property when the variable varies by one unit, p-values in brackets, not signifcant efffect are indicated as (n.s)).

Property	Intercept	Age	sex	Age·BMI	r
$\sigma_{\max}$	186.58	-1.0156	(n.s.)	(n.s.)	0.571
[MPa]	(< 0.0001)	(< 0.0001)	(n.s.)	(n.s.)	
$\sigma_{0.2}$	139.34	-0.4219	(n.s.)	(n.s.)	0.357
[MPa]	(< 0.0001)	(0.0047)	(n.s.)	(n.s.)	
$e_{\max}$	2.706	(n.s.)	(n.s.)	-6.2210^{-4}	0.447
[%]	(< 0.0001)	(n.s.)	(n.s.)	(< 0.0001)	
$W_{fracture}$	3.372	-3.0610^{-2}	(n.s.)	(n.s.)	0.438
[kJ/m^3]	(< 0.0001)	(< 0.0001)	(n.s.)	(n.s.)	

Our work finds a clear influence of age on failure stress ($p-$value < 0.0001), see table 3. Some earlier studies had not found such an influence because of various limitations, but this study and other recent similar studies strongly suggest that such an influence is present [13,14]. Indeed, an increase in the age of the individual leads to a reduction of the strength of its bone tissue. Additionally, age has a highly significant influence on the energy to fracture (SED), where a higher age entails a lower energy to fracture, and the same effect is corroborated in [13].

Moreover, an influence of age on ultimate strain was found, where the ultimate strain decreased as age increased. However, the ultimate strain was not only dependent on age, but also on the combination of BMI and age. Thus, it can be interpreted that an increase in BMI in an individual with a given age leads to a reduction of ultimate strain compared with an individual with the same age but lower BMI.

There are two possible explanations for the loss of mechanical capacity as age advances. On the one hand, a recent study of the same authors showed that Fractal Dimension of the medical images are higher for older people, this indicates that the occurrence of low bone mineral density is more prominent with age [14]. Possibly, this is associated both with decalcification of the cortical bone [24] and with alterations in the microstructure of the collagen matrix of the cortical bone [25].

On the other hand, yield strain and yield stress decrease with age, this maybe associated with a higher amount of cracking in cortical bone with age. The key to bone's brittleness is the strain and damage localization early which leads

to low post-yield strains and low-energy absorption to failure [26].

It is interesting to note that YM does not vary significantly with age. This would seem to imply that post-yield conditions are the responsible for the loss of mechanical capabilities, instead of a modification of pre-yield elastic behavior. In fact, there is still only limited understanding of the physics-based mechanisms of bone fracture and how they relate to its hierarchical, multidimensional structure [27–29].

Finally, no influence of age was observed on Young's modulus, interestingly, the most recent study, being similar to the present in number of samples, does not find that significant effect either [13], such parallel findings seems to corroborate the lack of significant effect.

No sex significant influence was found in any of the mechanical properties. A controlled sub-sample with a balanced number of females and males of the same age, revealed that no significant difference is present in our findings with respect to sex of the individual. Again, this lack of significant difference is found in a number of other studies [14,13]. The first two studies used small samples, but the last one, like the present study, did use a large sample, with conclusions identical to those found in this paper.

5 Conclusions

This study provides new methodological improvements for tensile testing on cortical bone coupons of human ribs. The use of these samples enables us to obtain direct values for the intrinsic material properties, isolating the material properties from the influence of geometrical characteristics of complete ribs.

83 coupons were obtained from $N = 64$ different donors, which provided a wide database of material properties for human rib cortical bone. The influence of anthropometric parameters on the material properties was determined.

The results indicate an overall average failure stress of 128.4±4.1 MPa, a yield strength of 115.5±3 MPa, a Young's modulus of 16±0.4 GPa and an ultimate strain of 1.72±0.12%.

An influence of age on most material properties was observed, except for Young's modulus. In all the affected properties, an increase in age led to a reduction of the mechanical property. A secondary influence of BMI was only observed for ultimate strain, with an increase of the BMI related to a decrease in this parameter, but only when the BMI is controlled by age. For the sex variable, no significant effect has been detected on any of the mechanical properties studied.

References

[1] Page Y, Cuny S, Hermitte T, & Labrousse M. (2012) "A comprehensive overview of the frequency and the severity of injuries sustained by car occupants and subsequent implications in terms of injury prevention", *Ann Adv Automot Med* **56**: 165.

[2] Cavanaugh, J. M. (2002). "Accidental injury: biomechanics and prevention", *Biomechanics of Thoracic Trauma*, Chapter 16, Springer, 374–404.

[3] Rebollo-Soria MC, Arregui-Dalmases C, Sánchez-Molina D, Velázquez-Ameijide J, & Galtés I (2016). "Injury pattern in lethal motorbikes-pedestrian collisions, in the area of Barcelona, Spain", *Journal of forensic and legal medicine*, **43**: 80–84.

[4] Weaver, A. A., Schoell, S. L., Talton, J. W., Barnard, R. T., Stitzel, J. D., & Zonfrillo, M. R. (2018). "Functional outcomes of thoracic injuries in pediatric and adult occupants", *Traffic Inj Prev*, **19**(sup1):S195.

[5] Cowin SC (2001).: "Bone mechanics handbook." *CRC press*.

[6] Burstein, A. H., Reilly, D. T., & Martens, M.: "Aging of bone tissue: mechanical properties", *Journal of Bone and Joint Surgery*, **58** (1), pp. 82–86, 1976.

[7] McCalden, R. W., McGeough, J. A., & Barker, M. B.: "Age-related changes in the tensile properties of cortical bone. The relative importance of changes in porosity, mineralization, and microstructure.", *Journal of Bone and Joint Surgery*, **75** (8), pp. 1193–1205, 1993.

[8] Mendizabal, A. (2010).: "Finite Element Simulation: Tensile test of rib cortical bone". *Chalmers University of Technology*.

[9] Caeiro, J. R., González, P., & Guede, D. (2013).: "Biomecánica y hueso (y II): ensayos en los distintos niveles jerárquicos del hueso y técnicas alternativas para la determinación de la resistencia ósea." *Revista de Osteoporosis y Metabolismo Mineral*, **5** (2), pp. 99–108.

[10] Yoganandan, N., & Pintar, F. A. (1998).: "Biomechanics of human thoracic ribs.", *Journal of biomechanical engineering*, **120**(1), pp. 100–104.

[11] Kalra, A., Saif, T., Shen, M., Jin, X., Zhu, F., Begeman, P., King, H. & Millis, S. (2015).: "Characterization of human rib biomechanical responses due to three-point bending.", *SAE Technical Paper*.

[12] Schafman, M.A., Kang, Y.-S., Moorhouse, K., White, S.E., Bolte IV, J.H. & Agnew, A.M. (2016).: "Age and sex alone are insufficient to predict human rib structural response to dynamic AP loading.", *Journal of biomechanics*, **49**, pp. 3516–3522.

[13] Katzenberger, M. J., Albert, D. L., Agnew, A. M., & Kemper, A. R. (2020).: "Effects of sex, age, and two loading rates on the tensile material properties of human rib cortical bone", *Journal of the mechanical behavior of biomedical materials*, 102, 103410.

[14] Velázquez-Ameijide J, García-Vilana S, Sánchez-Molina D, Llumà-Fuentes J, Martínez-González E, Rebollo-Soria MC, & Arregui-Dalmases C (2020): "Prediction of mechanical properties of human rib cortical bone using fractal dimension". *Computer Methods in Biomechanics and Biomedical Engineering*, 1–11.

[15] Kemper, A.R., McNally, C., Pullins, C.A., Freeman, L.J., Duma, S.M., Rouhana, S.W., (2007).: "The biomechanics of human ribs: material and structural properties from dynamic tension and bending tests", *Stapp Car Crash Journal* **51**:235–273.

[16] Pelker, R. R., Friedlaender, G. E., Markham, T. C., Panjabi, M. M., & Moen, C. J.: "Effects of freezing and freeze-drying on the biomechanical properties of rat bone". *Journal of Orthopaedic Research*, **1**(4), 405–411, 1983.

[17] Borchers, R. E., Gibson, L. J., Burchardt, H., & Hayes, W. C..: "Effects of selected thermal variables on the mechanical properties of trabecular bone". *Biomaterials*, **16**(7), 545–551, 1995.

[18] Sanchez-Molina, D., Velazquez-Ameijide, J., Quintana, V., Arregui-Dalmases, C., Crandall, J. R., Subit, D., & Kerrigan, J. R.: "Fractal dimension and mechanical properties of human cortical bone". *Medical engineering & physics*, **35** (5), pp. 576–582, 2013.

[19] Frank, S., & Spolenak, R. (2008).: "Optical strain measurement by digital image analysis." (Matlab script) Laboratory for Nanometallurgy, Dept. of Materials, Zurich (http://www.mathworks.com/matlabcentral/leexchange/20438-optical-strain-measurement-by-digital-image-analysis).

[20] Stitzel, J. D., Cormier, J. M., Barretta, J. T., & Kennedy, E. A. (2003).: "Defining regional variation in the material properties of human rib cortical bone and its effect on fracture prediction", *Stapp car crash journal*, **47**, pp. 243.

[21] Cormier, J. M., Stitzel, J. D., Duma, S. M., & Matsuoka, F.: "Regional variation in the structural response and geometrical properties of human ribs." *Annual Proceedings/Association for the Advancement of Automotive Medicine*, **49** pp. 153, 2005.

[22] Kemper, A.R., McNally, C., Kennedy, E.A., Manoogian, S.J., Ratch, A.L., ng, T.P, & Matsuoka, F. (2015).: "Material properties of human rib cortical bone from dynamic tension coupon testing", *Stapp Car Crash J*, **49**(11), pp. 199–230.

[23] Hansen, U., Zioupos, P., Simpson, R., Currey, J. D., & Hynd, D. (2008).: "The effect of strain rate on the mechanical properties of human cortical bone", *Journal of biomechanical engineering*, **130**(1): 011011.

[24] Sevostianov, V. (2014).: "Evaluation of decalcification induced changes in bone strength using electrical conductivity measurements", *ASME 2014 International Mechanical Engineering Congress and Exposition*, American Society of Mechanical Engineers Digital Collection.

[25] Isaksson, H., Harjula, T., Koistinen, A., Iivarinen, J., Seppänen, K., Arokoski, J. P., & Helminen, H. J. (2010).: "Collagen and mineral deposition in rabbit cortical bone during maturation and growth: effects on tissue properties", *Journal of orthopaedic research*, **28**(12), pp. 1626–1633.

[26] Zioupos, P., Hansen, U., & Currey, J. D. (2008).: "Microcracking damage and the fracture process in relation to strain rate in human cortical bone tensile failure", *Journal of Biomechanics*, **41**(14), pp. 2932–2939.

[27] Rho, J.Y., Kuhn-Spearing. L., & Zioupos, P. (1998).: "Mechanical properties and the hierarchical structure of bone", *Med. Eng. Phys.*, **20**, pp. 92–102.

[28] Weiner, S., & Wagner, H.D. (1998).: "The material bone: structure mechanical function relations", *Annu. Rev. Mater. Sci.*, **28**, pp. 271–298.

[29] Launey, M. E., Buehler, M. J., & Ritchie, R. O. (2010).: "On the mechanistic origins of toughness in bone", *Annual review of materials research*, **40**, pp. 25–53.